Structure of *Synechococcus elongatus* [Fe_2S_2] Ferredoxin in Solution†

Bettina Baumann,‡,§ Heinrich Sticht,‡,|| Manuela Schärpf,‡ Martin Sutter,⊥ Wolfgang Haehnel,⊥ and Paul Rösch*,‡

Lehrstuhl für Biopolymere, Universität Bayreuth, Universitätsstrasse 30, D-95447 Bayreuth, Germany, and Lehrstuhl für Biochemie der Pflanzen, Institut für Biologie II, Albert-Ludwigs-Universität, Schänzlestrasse 1, D-79104 Freiburg, Germany

Received May 15, 1996; Revised Manuscript Received July 8, 1996⊗

ABSTRACT: Ferredoxins of the [Fe_2S_2] type function in photosynthetic electron transport as essential electron acceptors of photosystem I. The solution structure of the 97 amino acid ferredoxin from the thermophilic cyanobacterium *Synechococcus elongatus* was determined by nuclear magnetic resonance spectroscopy and restrained molecular dynamics calculations. The structure consists of a four-stranded parallel/antiparallel β-sheet, a short two-stranded antiparallel β-sheet, and three short helices. The overall structure is similar to the structure of the ferredoxin from *Anabaena*. In contrast to related ferredoxins from mesophilic organisms, this thermostable protein contains a salt bridge inside a 17-amino acid hydrophobic core.

Ferredoxin (Fd)[1] is an essential electron carrier transferring electrons from the membrane bound complex of photosystem I to the Fd:$NADP^+$ oxidoreductase (EC 1.18.1.2) which, in turn, reduces $NADP^+$ for CO_2 fixation in photosynthesis. Ferredoxin I in oxygenic, photosynthetic organisms is a soluble acidic protein with a [Fe_2S_2] center that transfers one electron, while in anoxygenic procaryotic organisms the major Fd is a [Fe_4S_4] protein (Knaff & Hirasawa, 1991). Cells with a deletion of the *petFI* gene encoding Fd I were not viable (van den Plas et al., 1988) showing that its function is indispensable. Fd is reduced by one of the two [Fe_4S_4] centers of the PsaC subunit at the stromal side of the photosystem I complex. This electron transfer is only possible on simultaneous contact with the positively charged PsaD subunit (Zanetti & Merati, 1987). The role of the peripheral PsaE subunit of photosystem I may be the stabilization of the electron transfer to Fd (Weber & Strotmann, 1993; Rousseau et al., 1993) or facilitation of the cyclic electron transfer (Yu et al., 1993). Fd I appears to serve a central role in shuttling the reducing equivalents originating from H_2O not only to the Fd:$NADP^+$ oxidoreductase, but also to other enzymes such as the fdx:nitrite oxidoreductase (EC 1.7.7.1), glutamate synthase (EC 1.4.7.1), sulfate reductase, or the Fd:thioredoxin reductase.

These multiple interactions suggest a docking site of Fd at these enzymes, possibly similar to a mirror-image structure of Fd contributing negatively charged groups for an electrostatically stabilized complex formation (Knaff & Hirasawa, 1991) while small differences may control the electron transfer channeled to the different pathways. Recently the structure of photosystem I from *Synechococcus elongatus* has been solved at 6 Å resolution (Krauss et al., 1993). Improvement of the structure may reveal details of the binding site of Fd (Fromme and Saenger, personal communication). Therefore, the structure of Fd from this organism is of particular interest.

In general, the known [Fe_2S_2] ferredoxins from plants, algae, and cyanobacteria consist of 93−99 amino acid residues (Matsubara & Saeki, 1992) and are highly homologous among each other (Table 1). The iron−sulfur clusters are attached to the protein chain via cystein residues. For example, in the 97-amino acid *S. elongatus* ferredoxin (Fd_{Se}) the [Fe_2S_2] cluster active in the electron transfer is attached to the protein chain via the sulfhydryl groups of Cys40, Cys45, Cys48, and Cys78 (Hase et al., 1983). Particularly the cluster surroundings are well conserved in the various ferredoxins (Fukuyama et al., 1980). This high sequence homology is even more remarkable considering the fact that the cyanobacteria were among the first photosynthetic organisms and thus have been around for more than three billion years (Meyer, 1988).

The crystal structure of four ferredoxins of the [Fe_2S_2] type from different organisms is known: Fukuyama et al. published the first crystal structure of Fd from *Spirulina platensis* (Fukuyama et al., 1980). Similar crystal structures have been found for *Aphanothece sacrum* (Tsukihara et al., 1990), *Anabaena* PCC 7120 (Rypniewski et al., 1991), and *Equisetum arvense* (Ikemizu et al., 1994). The nuclear magnetic resonance structure of the [Fe_2S_2] Fd from *Synechocystis* sp. PCC 6803 (Lelong et al., 1995) and of putidaredoxin from *Pseudomonas putida* (Pochapsky et al., 1994), which is only distantly related to the cyanobacterial ferredoxins, were recently determined. In addition, the ^1H,

† Support by Deutsche Forschungsgemeinschaft SFB 388/A1 is gratefully acknowledged. The atomic coordinates (code 1ROE) have been deposited in the Protein Data Bank, Brookhaven National Laboratory, Upton, NY.

* To whom correspondence should be adressed: Tel: ++49 921 553540. Fax: ++49 921 553544. E-mail: paul.roesch@uni-bayreuth.de.

‡ Universität Bayreuth.

§ Present address: Institut für Organische Chemie, Johann-Wolfgang-Goethe-Universität Frankfurt, Marie-Curiestrasse 11, D-60439 Frankfurt, Germany.

|| Present address: Department of Biochemistry, University of Oxford, South Parks Road, Oxford OX1 3QU, England.

⊥ Albert-Ludwigs-Universität.

⊗ Abstract published in *Advance ACS Abstracts,* September 1, 1996.

[1] Abbreviations: 2D, two dimensional; clean-TOCSY, TOCSY with suppression of NOESY-type crosspeaks; COSY, correlated spectroscopy; DQF-COSY, double quantum filtered COSY; DSS, 2,2-dimethyl-2-silapentane-5-sulfonic acid; DSSP, definition of secondary structure of proteins; Fd, ferredoxin; Fd_{Se}, *Synechococcus elengatus* [Fe_2S_2] ferredoxin; MD, molecular dynamics; NMR, nuclear magnetic resonance; NOE, nuclear Overhauser effect; NOESY, NOE spectroscopy; ppm, parts per million; RMSD, root mean square deviation; SA, simulated annealing; TOCSY, total correlation spectroscopy; TPPI, time proportional phase incrementation.

S0006-2960(96)01144-0 CCC: $12.00

Table 1: Sequence Alignment of Ferredoxins[a]

```
Species                 10        20        30        40
                        |         |         |         |
SYN.ELONGATUS     AT-YKVTLVR-PDGSETTIDVPEDEYILDVAEEQGLDLPFSCRAGACSTC
ANA.PCC7120       AT-FKVTLINEAEGTSNTIDVPDDEYILDAAEEQGYDLPFSCRAGACSTC
SPI.PLATENSIS     AT-YKVTLINEAEGINETIDCDDDTYILDAAEEAGLDLPYSCRAGACSTC
DUN.SALINA        S--YMVTLK--TPSGEQKVEVSPDSYILDAAEEAGVDLPYSCRAGSCSSC
EQU.ARVENSE       A--YKTVLK--TPSGEFTLDVPEGTTILDAAEEAGYDLPFSCRAGACSSC
ORY.SATIVA        AT-YNVKLI--TPDGEVELQVPDDVYILDQAEEEGIDLPYSCRAGSCSSC
PHY.AMERICANA     AT-YKVTLV--TPSGTQTIDCPDDTYVLDAAEEAGLDLPYSCRAGSCSSC
RAP.SATIVUS       SAVYKVKLI-GPDGQENEFDVPDDQYILDAAEEAGVDLPYSCRAGACSTC
SPI.OLERACEA      AT-YKVTLV--TPSGSQVIECGDDEYILDAAEEKGMDLPYSCRAGACSSC
                  .  .   *          .   .  .** *** * ***.*****.**.*

Species           50        60        70        80        90
                  |         |         |         |         |
SYN.ELONGATUS     AGKLLEGEVDQSDQSFLDDDQIEKGFVLTCVAYPRSDCKILTNQEEELY-
ANA.PCC7120       AGKLVSGTVDQSDQSFLDDDQIEAGYVLTCVAYPTSDVTIQTHKEEDLY-
SPI.PLATENSIS     AGTITSGTIDQSDQSFLDDDQIEAGYVLTCVAYPTSDCTIKTHQEEGLY-
DUN.SALINA        AGKVESGTVDQSDQSFLDDDQMDSGFVLTCVAYATSDCTIVTHQEENLY-
EQU.ARVENSE       LGKVVSGSVDESEGSFLDDGQMEEGFVLTCIAIPESDLVIETHKEEELF-
ORY.SATIVA        AGKVVSGEIDQSDQSFLDDDQVAAGWVLTCHAYPKSDIVIETHKQEDLI-
PHY.AMERICANA     TGKVTAGTVDQEDQSFLDDDQIEAGFVLTCVAFPKGDVTIETHKEEDIV-
RAP.SATIVUS       AGKIEKGQVDQSDGSFLEDHHFEKGYVLTCVAYPQSDLVIHTHKEEELF-
SPI.OLERACEA      AGKVTSGSVDQSDQSFLEDGQMEEGWVLTCIAYPTGDVTIETHKEEELTA
                   * .  * .*. . ***.* .   * **** * . .*  * *...* .
```

[a] Sequence alignment of $[Fe_2S_2]$-ferredoxins from blue-green algae (*Synechococcus elongatus, Anabaena PCC7120, Spirulina platensis*), a green alga (*Dunaliella salina*), and plants (*Equisetum arvense, Oryza sativa, Phytolacca americana, Raphanus sativus, Spinacia oleracea*). The numbering scheme of Fd_{Se} is given at the top. The four cluster-ligating cysteines are in bold. "*" designates conserved amino acids, "." designates conservative replacements. Sequences as deposited in the SWISS-PROT data bank. The alignment was performed with the Clustal V program using standard parameters (Higgins et al., 1992).

^{13}C, and ^{15}N resonances of double-labeled *Anabaena* ferredoxin were assigned (Oh & Markley, 1990).

All of these proteins are from mesophilic bacteria. In contrast, *S. elongatus* is a thermophile, and the structure of the $[Fe_2S_2]$ ferredoxin of this organism has been demonstrated to reamain intact at temperatures of up to 333 K (Koike & Katoh, 1979). Thus, our purpose in determining the solution structure of the Fd_{Se} was 2-fold: First, we wanted to determine the structure of a ferredoxin in an electron transfer pathway whose main component, photosystem I, is currently under structural investigation; second, we wanted to determine the structure of a thermostable protein whose thermolabile counterparts are structurally well-known from crystal analyses and, in recent studies, also from NMR spectroscopy (Lelong et al., 1995).

EXPERIMENTAL PROCEDURES

Culture. The thermophilic unicellular cyanobacterium *S. elongatus* was grown at 57 °C in 20 l flasks in the inorganic medium D of Castenholz (Castenholz, 1969), after adding 0.5 g of $NaHCO_3$/L of medium according to Schatz and Witt (1984). The culture was bubbled with air enriched with 4% by volume CO_2 and illuminated with fluorescent lamps Osram Universal White light (light color 25). During the growth period of 7 days, the amount of air was increased stepwise from 30 to 120 L/h and the intensity of illumination was increased from 3 to 25 W/m^2. The cells were harvested at the late exponential phase by centrifugation and stored at −80 °C.

Isolation and Purification of Fd. The isolation of Fd followed the procedure described by Shin et al. (1984). The eluted Fd fractions from the Toyopearl HW-65C column were concentrated using a pressure dialysis cell fitted with a YM-5 membrane (Amicon) and desalted by gelfiltration with a PD-10 column (Pharmacia). For further purification Fd was loaded on a DE-52 (Whatman) column (12 cm × 3 cm ∅), equilibrated with 10 mM sodium phosphate, pH 7.5, containing 0.2 M sodium chloride and eluted with a linear gradient of 200−500 mM sodium chloride in phosphate buffer. Fractions containing Fd were concentrated and desalted as described above, loaded on an anion exchange column of 1 mL (Hi-Trap-Q, Pharmacia), equilibrated with 20 mM Tris, pH 7.5, and eluted with a linear gradient of 0−500 mM sodium chloride in the Tris buffer. The purest Fd fractions with an absorption ratio of $A_{423.5}/A_{276} = 0.65$ were concentrated and desalted again. The integrity of the sample with respect to the contents of the $[Fe_2S_2]$ cluster was checked by UV/vis spectroscopy using the cluster-typical peaks at 331, 423.5, and 463.5 nm as indicators.

Mass Spectrometry. The molecular mass was determined with a tandem quadrupole (MS/MS) mass spectrometer TSQ700 (Finnigan MAT; San Jose, CA) equipped with an interface for electrospray ionization (Edmonds & Smith, 1990) and controlled by a DEC 5000 computer. The protein solution was applied with a sample loop and a syringe pump at a flow rate of 5 mL min^{-1}. The molecular mass M is calculated from the average over a series of peaks observed at increasing values of m/z for the protein molecule associated with a decreasing number z of protons, $M = (m/z - 1)z$. The spectra were deconvoluted with the program BIOMASS and analyzed by the centroid mode.

NMR Spectroscopy. The NMR sample contained 5.5 mM Fd in 50 mM sodium phosphate buffer (pH 7.0), containing 10% (v/v) D_2O as a spin lock signal. Samples for the measurements in D_2O were prepared by dissolving the lyophilized protein in 0.5 mL of D_2O (99.994 atom %, Sigma, Deisenhofen, Germany). All NMR experiments were carried out on a Bruker AMX 600 spectrometer with standard methods (Wüthrich, 1986; Ernst, 1992). In H_2O/D_2O (9:1) the following experiments were measured: double-quantum filtered correlation spectrum (DQF-COSY) at $T = 288$, 298 K, and 313 K, total correlation spectrum (clean-TOCSY, spin-lock field of approximately 12 kHz) at $T = 288$, 298, and 313 K, mixing time 80 ms, at $T = 313$ K, mixing time 150 ms; nuclear Overhauser enhancement spectrum (NOESY) at $T = 288$, 298, and 313 K, mixing time 200 ms, and at $T = 313$ K, mixing time 100 ms.

DQF-COSY, clean-TOCSY (mixing time 80 ms), and NOESY (mixing time 200 ms) spectra were also obtained at $T = 298$ K in D_2O. The quality of the spectra was best at $T = 298$ K, so that the resonance assignments were based mainly on spectra obtained at this temperature.

The spectra were acquired in the phase-sensitive mode with quadrature detection in both dimensions, using the time-proportional phase incrementation technique (Marion & Wüthrich, 1983). The solvent signal was suppressed by continuous coherent irradiation prior to the first excitation pulse and during the mixing time of the NOESY experiments.

All spectra were recorded with a spectral width of 7692 Hz in both dimensions and 4k × 0.5k time domain data points. A sine bell-squared filter with a phase shift of $\pi/4$ was used prior to Fourier transformation. Application of zero-filling resulted in a data size of 4k × 1k frequency domain data points. After Fourier transformation, a seventh-order base line correction with sine and cosine functions (Güntert & Wüthrich, 1992) was applied. The sample temperature was regulated using a standard Bruker VT2000 temperature control unit with a continuous stream of cooled, dried air. In addition to the standard Bruker spectrometer control software, the NDEE software package was used for data processing on X-window workstations (Software Symbiose, Inc., Bayreuth, Germany). Chemical shift values are reported in ppm from 2,2-dimethyl-2-silapentanesulfonate.

Distance information was obtained from two-dimensional NOESY spectra at T = 298 K in H_2O/D_2O (9:1) with mixing times of 200 ms, since the 100 ms and the 200 ms spectra were apparently identical. NOESY cross-peak intensities were grouped into three distance categories according to their relative intensities: strong, 0.18−0.29 nm; medium, 0.18−0.42 nm; weak, 0.18−0.57 nm. Peak intensities were estimated from the number of contours in contour plots of NOESY spectra. For distance limits involving non-stereospecifically assigned methylene protons, pseudoatom corrections of 0.05 nm were added (Wüthrich et al., 1983). Taking into account the apparent higher intensity of methyl resonances, 0.05 nm was added to distances involving methyl groups (Wagner et al., 1987; Clore et al., 1987). Coupling constants were measured between the antiphase peaks of the resonances in the COSY spectra (Neuhaus et al., 1985). Deviations of 30° from the measured angle were allowed without penalty in the calculation.

For the unambiguous assignment of frequency-degenerated NOEs an iterative approach was used similar to the strategy described by Kraulis et al. (1989). Degenerate NOESY cross-peaks were allowed to enter the calculation only after they had been verified in at least 50% of crudely defined structures calculated from unambiguous data. Mutual proton distances were identified in these structures making use of the back-calculation subroutine of the NDEE program package.

Hydrogen bonding restraints were deduced from the interpretation of COSY spectra that were collected from samples that had been lyophilized and redissolved in 99.994% D_2O twice. A slow amide proton exchange was taken as indicative of a proton involved in a hydrogen bond (Wüthrich, 1986).

Modeling of the [Fe_2S_2] Cluster and Its Environment. NMR studies of *Anabaena* Fd (Oh & Markley, 1990) revealed that protons in a distance of less than 0.78 nm from the iron atoms of the cluster are not detectable in 2D-NMR spectra, rendering a modeling of this region necessary. The modeling followed an approach that was recently described by Pochapsky et al. (1994) and also successfully applied for the structure determination of the [Fe_2S_2] Fd from *Synechocystis* (Lelong et al., 1995). This approach is based on the observation that the structure of the [Fe_2S_2] cluster and its environment is highly invariant in all [Fe_2S_2] ferredoxins (Lelong et al., 1995).

The distance and dihedral angle restraints were obtained from analysis of [Fe_2S_2] Fd structures determined by X-ray crystallography (Brookhaven Protein Data Base accession code given in parentheses): *Spirulina platensis* (3FXC; Tsukihara et al., 1981); *Aphanotece sacrum* (1FXI; Tsukihara et al., 1990); *Anabaena* 7120 (1FXA; Rypniewski et al., 1991), and *Equisetum arvense* (1FRR; Ikemizu et al., 1994). To take into account the conformational freedom of the protein appropriately, deviations of ±0.05 nm from the derived distances and of ±30° from the derived dihedral angles were allowed without penalty in the molecular dynamics calculation. All restraints are summarized in Table 2, parts B and C.

Molecular Dynamics Calculations. The X-PLOR 3.1 package (Brünger, 1993) was used to calculate three-dimensional structures. The standard protocols for *ab initio* simulated annealing (SA) and SA refinement were applied with some minor modifications described below. The initial structure calculations started from an extended template with a satisfactory local geometry. At this stage of the calculations, 1339 unambigous NOEs (579 inter-residual, 760 intra-residual) were used as distance restraints, supplemented by 34 restraints for the cluster and its environment.

In order to remove some close nonbonded contacts, 200 cycles of unrestrained energy minimization were carried out using the Powell algorithm (Powell, 1977). In the SA procedure, 75 ps of molecular dynamics were calculated at 1000 K, the final 25 ps with an increased weight on geometry

Table 2: Restraints Used for the Structure Calculation[a]

A. Experimental Restraints for the Final Structure Calculation	
total no. of experimental restraints	1784
total no. of NOE restraints	1720
intraresidual NOEs $\|i - j\| = 0$	759
sequential NOEs $\|i - j\| = 1$	434
medium-range NOEs $\|i - j\| = 2, 3, 4, 5$	173
long-range NOEs $\|i - j\| > 5$	354
hydrogen bonds	28
dihedral angle restraints	36
B. Derived Angle Restraints	
residue	φ/ψ (deg)
39	−133/−76
40	−74/−29
41	53/25
42	−137/21
43	73/16
44	−120/20
45	−144/−170
46	−120/3
47	−53/−49
48	−74/−4
76	−96/103
77	−58/−25
78	−71/−14
79	−131/20
C. Derived Distance Restraints	
bond	bond length (nm)
Fe−S	0.225
Fe−S_γ(Cys)	0.220
bond angle type	bond angle (deg)
Fe−S−Fe	75.0
S−Fe−S	105.0
Fe−S_γ−C_β(Cys)	109.5
conserved distance	distance (nm)
C_α(Cys40)−C_α(Cys45)	0.67 ± 0.05
C_α(Cys40)−C_α(Cys48)	0.90 ± 0.05
C_α(Cys40)−C_α(Cys78)	0.86 ± 0.05
C_α(Cys45)−C_α(Cys48)	0.75 ± 0.05
C_α(Cys45)−C_α(Cys78)	0.99 ± 0.05
C_α(Cys48)−C_α(Cys78)	0.62 ± 0.05

[a] Overview of the kind and number of restraints used for the final structure determination. NOEs were represented by a single distance restraint as described in the text. For each hydrogen bond two separate distance restraints were included: d_{NH-O} = 0.17−0.23 nm, d_{N-O} = 0.24−0.33 nm. The data given in B and C were derived from the crystal structures of homologous ferredoxins as described in Experimental Procedures. Deviations of ±0.05 nm from the derived distances and of ±30° from the derived dihedral angles were allowed without penalty in the molecular dynamics calculation.

and an asymptote with a steeper slope. Electrostatic and hydrogen bonding interactions were not incorporated explicitly, and the van der Waals interactions were described by a simplified repulsive ("repel") energy term. For the NOE effective energy term representing the interproton distances a soft square-well potential function was applied (Nilges et al., 1988a). The system was cooled to 100 K in 60 ps followed by 500 cycles of energy minimization. A time step of 3 fs was applied throughout the protocol.

Restraints for hydrogen bonds were deduced from the 20 resulting crudely defined structures that were calculated without explicit hydrogen bonds.

Hydrogen bond restraints were introduced into the structure calculation if two criteria were met: A slow exchange of the corresponding amide proton and an N−H···O distance of less than 0.23 nm in at least 70% of the calculated structures. The N-H···O angle was not considered at this stage of the calculation, but measuring the H···O instead of the N···O distance avoids the identification of hydrogen

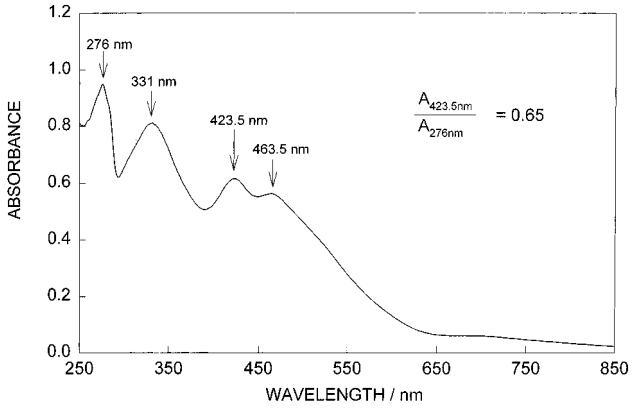

FIGURE 1: UV/Vis-absorption spectrum of oxidized ferredoxin from *S. elongatus* in 20 mM sodium phosphate buffer pH 7.0. The spectrum was recorded on an UVPC 2101 spectrophotometer (Shimadzu) with automatically calibrated wavelength accuracy. The spectral bandwidth was 0.2 nm at automatical data aquisition and medium scan speed.

bonds with an unfavorable geometry. For each backbone hydrogen bond two restraints were included in the calculations: d_{NH-O} = 0.17−0.23 nm, d_{N-O} = 0.24−0.33 nm (Kraulis et al., 1989). The experimental restraints used for the final structure calculation are summarized in Table 2 (part A).

After the assignment of the ambiguous NOEs, the final calculations were carried out as described above for the initial structure calculations, with some minor modifications. The cooling stage of the *ab initio* simulated annealing comprised 80 ps of molecular dynamics. Timesteps of 2.5 fs (high-temperature phase) and 1 fs (cooling phase) were applied.

A protocol of the slow-cooling type was used for the refinement. The system was cooled from 1000 to 100 K within 80 ps employing a 1 fs time step. The NOE effective energy term was represented by a square-well potential function.

Of the resulting 50 structures those 20 structures with the lowest internal energy and the smallest number of violations of the experimental data were selected for further characterization.

RESULTS AND DISCUSSION

UV/Vis and Mass Spectrometry. The ferredoxin from *S. elongatus* used for the NMR studies was characterized by UV/vis (Figure 1) and mass (Figure 2) spectrometry. The UV/vis spectra clearly showed three peaks characteristic of the presence of the [Fe_2S_2] cluster at 331, 423.5, and 463.5 nm, and the mass spectrum monitored in the presence of 25% methanol and 0.5% acetic acid confirmed the mass of the purified product to be 10 715.7 in excellent agreement with the mass of 10 715.8 expected for the apoprotein (Hase et al., 1983), while in the presence of 50% acetonitril and 0.1% trifluoracetic acid the mass of 10,713.4 (not shown) suggests the oxidation of two Cys residues.

Resonance Assignments. Sequence specific resonance assignments were performed according to standard methods (Wüthrich, 1986; Englander & Wand, 1987). Identification of spin systems was obtained from DQF-COSY and clean-TOCSY spectra. Through-space connectivities were deduced from NOESY spectra in H_2O/D_2O (9:1) and in D_2O, respectively. The typical spectral quality can be estimated from the NOESY spectrum shown in Figure 3. Frequency-

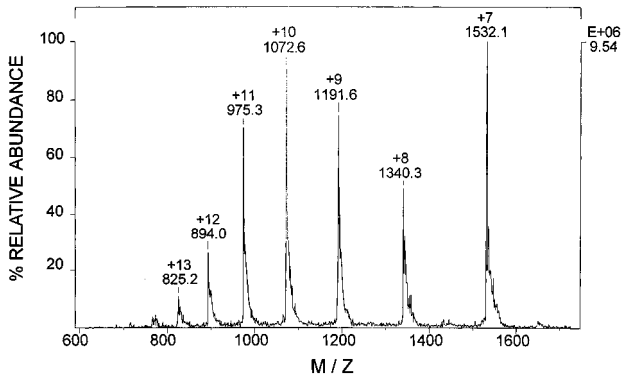

FIGURE 2: Electrospray mass spectrum of ferredoxin from *S. elongatus* with positive mode ionization. The mass spectrum was recorded on a electrospray TSQ 700 mass spectrometer (Finnigan). About 1 nmol of protein dissolved in 1:1 25% (v/v) methanol/0.5% (v/v) acetic acid was injected.

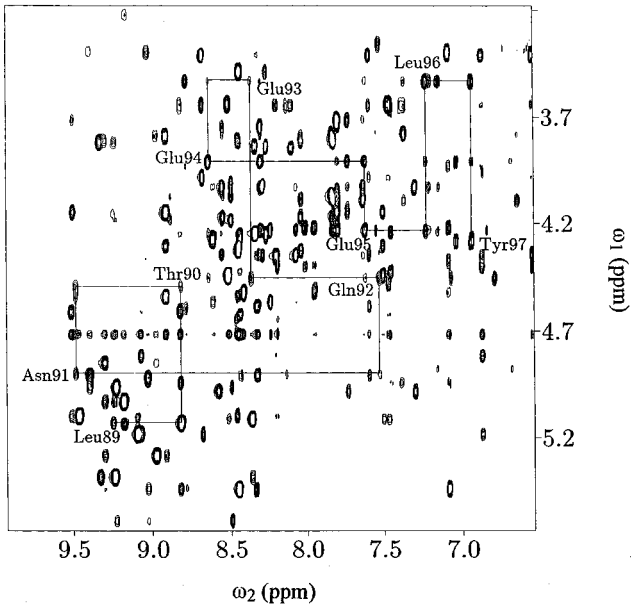

FIGURE 3: Fingerprint region of a NOESY spectrum of Fd_{Se}. The backbone chain tracing from Leu89 to Tyr97 is indicated by lines. The spectrum was recorded with a mixing time of 200 ms at 298 K, pH 7.0, in H_2O/D_2O (9:1). All chemical shifts are reported in ppm from DSS.

degenerated NOEs used for the sequence-specific assignment procedure were distinguished in NOESY spectra measured at different temperatures. Additional information could be obtained from analysis of the effects arising from the paramagnetic cluster: Unusual line-broadening and shift effects were attributed to the spatial proximity of the corresponding protons to the iron−sulfur cluster. Examples are Leu65 and Ala80, whose amide protons are shifted to low field (Leu65: 10.41 ppm) and high field (Ala80: 6.29 ppm), respectively. In cases which were still ambiguous, it proved to be very helpful to resort to the assignments published for the homologous *Anabaena* PCC7120 ferredoxin (Oh & Markley, 1990). As a result of these procedures, 79 out of the total of 97 amino acids could be assigned. (The resonance assignments of Fd_{Se} at pH 7.0, 298 K, are noted in the supporting information.) No resonances could be found originating from sequence regions from Phe38 to Ala49 and Leu76 to Val79 as well as from Gln62 and Phe64, and the resonances from Ser63 were unusually broadened and weak. Indeed, the absence or low intensity of these

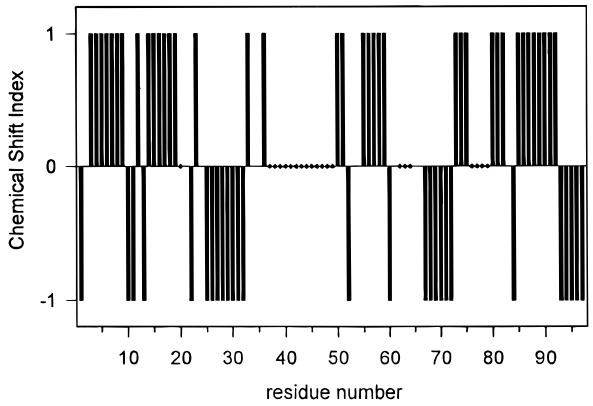

FIGURE 4: Chemical shift diagram of Fd_{Se} according to the procedure of Wishart et al. (1992). Deviations from the "random coil" chemical shifts are indicated by bars if they exceed a value of more than ±0.1 ppm for the shift of the C_α-protons. Diamonds mark residues with unassigned C_α-proton resonances. Helical regions correspond to negative chemical shift indices, and β-sheets correspond to positive chemical shift indices.

resonances could be attributed to their spatial proximity to the $[Fe_2S_2]$ cluster: Phe38 to Ala49 and Leu76 to Val79 contain all cluster-ligating cysteine residues, and Gln62 to Phe64 is known to be close to the cluster in the crystal structure of the *Anabaena* 7120 protein (Rypniewski et al., 1991). These regions also remained unassigned in the NMR studies of *Anabaena* (Oh & Markley, 1990) and *Synechocystis* Fd (Lelong et al., 1995). Surprisingly, the SH proton of Cys86 could be clearly observed in Fd_{Se}, although observation of this proton type is usually strongly hampered by chemical exchange with the solvent.

Analysis of $C_\alpha H$ Shift Patterns. Analysis of the $C_\alpha H$ chemical shifts according to Wishart et al. (1991, 1992) usually gives a first estimate on the secondary structure contents of proteins. The chemical shift index plot as in Figure 4 suggests that most of the amino acids of Fd_{Se} are involved in the formation of regular secondary structure. In particular, the plot suggests that amino acids 3−9, 14−19, 55−59, 73−75, 80−82, and 85−92 form β-strand type structures, whereas 25−32, 67−72, and 93−97 are involved in α-helix formation.

Proton/Deuteron Exchange Experiments. After 2-fold exchange of the labile protons in D_2O, it was found that the amide protons of Val5, Thr6, Leu7, Val8, Ile17, Val19, Glu23, Val28, Lys51, Asp58, Val75, Tyr81, Arg83, Ser84, Cys86, Ile88, and Leu89 were slowly exchanging.

NOE Statistics. After verification of ambiguous NOEs as described in above a total of 759 intraresidual and 961 interresidual NOEs could be assigned, corresponding to an average of 9.6 intraresidual and 12.2 interresidual NOEs per assigned residue (Figure 5). Except for the nonassigned regions in the cluster vicinity, the deviation of the number of NOEs from the average number is low, indicating that the protein possesses an overall compact structure. A plot of sequential and medium-range NOEs (Figure 6) further clarifies type and location of helical secondary structure by its typical $C_\alpha H$-NH(i,i+3) and $C_\alpha H$-$C_\beta H$(i,i+3) NOEs. This plot indicates that helical secondary structure is present in regions 24−34, 65−75, and 93−97. Inspection of the NOE contact map (Figure 7) additionally suggests presence of an antiparallel β-sheet between strands 3−9 and 14−20, a parallel β-sheet between strands 3−9 and 85−92, and an antiparallel β-sheet between 50−60 and 82−92.

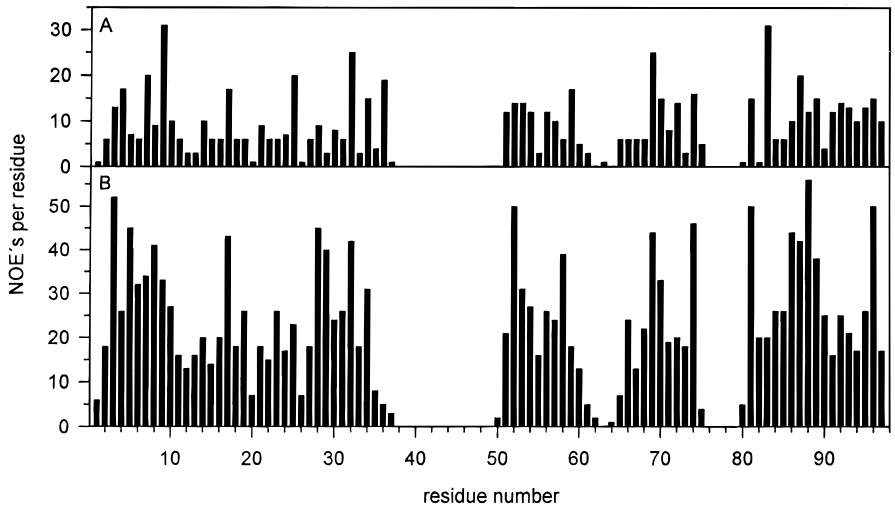

FIGURE 5: Number of intraresidual (A) and interresidual (B) NOEs that were assigned from NMR spectra versus the Fd_{Se} amino acid seqence. The lack of NOEs in the sequence regions from residues 38−49 and residues 76−79 is a consequence of the spatial proximity to the cluster.

FIGURE 6: Pattern of NOESY cross-peaks as derived from the NOESY spectra with 200 ms mixing time. The relative intensity of the cross-peaks is indicated by the width of the bars in the diagram. The $C_\alpha H-NH$ (i,i+3) and $C_\alpha H-C_\beta H$ (i,i+3) cross-peak pattern clearly delineates three helical regions. $^3J_{HN_\alpha}$ coupling constants were divided into three groups according to their magnitude: $J < 6$ Hz (●), 6 Hz $< J <$ 9 Hz (◆), and $J \geq 9$ Hz (■).

Analysis of $^3J_{HN_\alpha}$ Coupling Constants. A high number of $^3J_{HN_\alpha}$ coupling constants showed values above 9 Hz, indicative of β-type structures (Figure 6). These coupling constants were used as dihedral angle restraints in the final structure calculations. In contrast, only one of the $^3J_{HN_\alpha}$ coupling constants we could measure was below 6 Hz.

Description of the Structure. None of the 20 structures that were selected after the molecular dynamics calculations showed distance violations of more than 55 pm or dihedral angle violations of more than 4° both for NMR-derived restraints and restraints derived from homologous ferredoxin structures. The 20 selected structures showed a low overall RMSD value of 0.087 nm for the backbone atoms and of 0.130 nm for all heavy atoms, respectively (Table 3).

The overlay of the backbone atoms of the ten best structures resulting from the restrained MD calculations displays the excellent agreement between these structures with the exception of the regions close to the $[Fe_2S_2]$ cluster and the loop region from Ser60 to Phe64 (Figure 8). The former was modeled from X-ray crystallographic data with very conservative restraints, whereas no restraints for the region Gln62-Phe64 were introduced. This latter region was not visible from in the 2D-NMR spectra or exhibits broadened resonances, and may thus be close to the cluster as was observed in the X-ray structure of the homologous protein from *Anabaena* (Rypniewski et al., 1991). The elements of regular protein secondary structure as defined by the DSSP program (Kabsch & Sander, 1983) from the final, restrained MD calculated structure, are in excellent agreement with the secondary structure elements suggested from the NOE pattern (Figure 7) and the chemical shift indexing procedure (Figure 4). One representative structure, that was derived from the molecular dynamics calculations is shown in Figure 9. The protein consists of an extended, four-stranded β-sheet and a short two-stranded β-sheet (Figure 10A). Tyr3-Leu7 forms an antiparallel sheet with

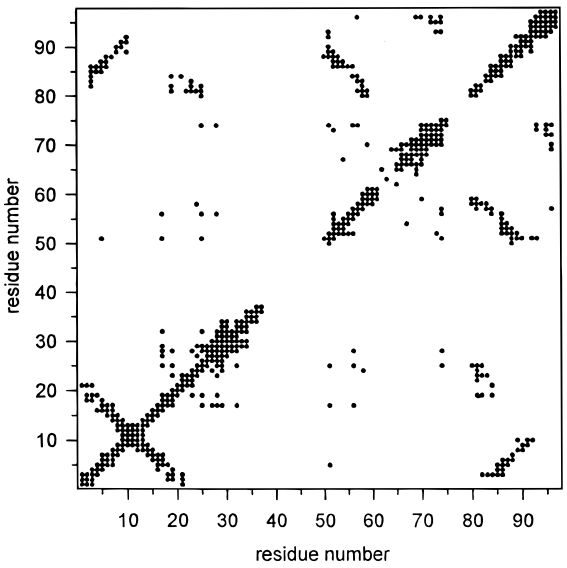

FIGURE 7: Summary of the spatial interactions between the amino acids of Fd_{Se}. Dots in the matrix plot represent NOEs that were observed between the corresponding residues. The length and position of the helices and β-sheets can be deduced from this presentation.

Table 3: Molecular Dynamics Statistics[a]

average energies (E, kJ/mol)	
total	8942 ± 236
bonds	669 ± 43
angle	2700 ± 79
impropers	519 ± 39
van der Waals	1881 ± 144
NOE	3168 ± 71
dihedral angle	5 ± 2
electrostatic	-9168 ± 334
RMS deviations from idealized distances (pm)	
NOE	8.7 ± 0.10
bonds	0.9 ± 0.03
RMS deviations from idealized angles (deg)	
bond angles	1.26 ± 0.02
impropers	1.05 ± 0.04
dihedral angles	0.12 ± 0.02
RMSD among structures (nm)	
backbone heavy atoms	0.087
all heavy atoms	0.130

[a] Energy contributions to the structure and deviations from standard geometry. E_{VDW}, van der Waals energy; E_{NOE}, effective NOE energy term. The energy values reported here result from the target function used for the MD calculations as described in the text. The electrostatic energy (E_{elec}) term was not included in the target function. It is calculated as an independent check to prove the validity of the structure determination procedure (Nilges et al., 1988b). All values are mean values over 20 refined structures. Values in parentheses indicate the standard deviations from this mean.

Thr15-Val19, connected by a loop, Val8-Glu14. Lys4-Val8 and Cys86-Thr90 form a parallel β-sheet, whereas Ile88-Thr90 and Gly50-Leu52 form the fourth short antiparallel β-strand. An additional second antiparallel β-sheet is formed by residues Glu56-Asp58 and Tyr81-Arg83.

The hydrogen bond pattern for this β-sheet region was confirmed by observation of slow proton-deuteron exchange for all amide protons involved in hydrogen bonds according to the scheme in Figure 10B except for the terminal hydrogen bonds involving the amide protons of Tyr3, Thr15, and Thr90. This observation underlines the high intrinsic stability of this structural element.

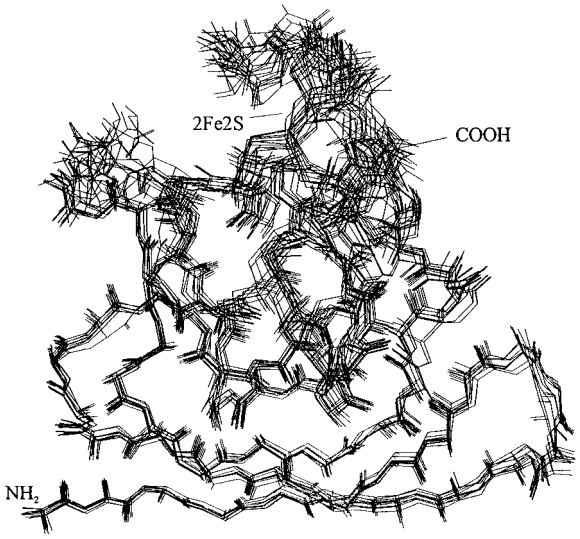

FIGURE 8: Superposition of ten backbone structures of Fd_{Se}. The ten structures were obtained from restrained MD calculations and showed the lowest internal energy and the smallest number of violations of the experimental data.

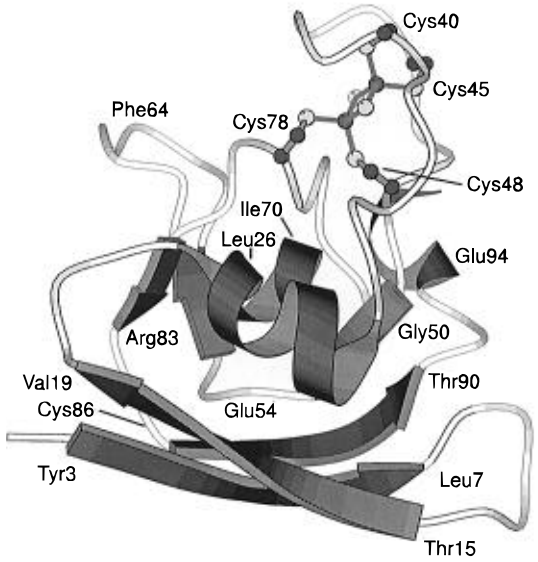

FIGURE 9: MOLSCRIPT (Kraulis, 1991) schematic presentation of the Fd_{Se} structure. For clarity, the same orientation as in Figure 8 was chosen and a subset of the amino acid positions is labeled. The iron−sulfur cluster and the ligating cysteines are shown in ball and stick representation.

The 20 structures selected after the final stages of the restrained MD calculations were analyzed for hydrogen bonds. The excellent quality of the calculated structures allowed consideration of the N−H···O angle in addition to the donor−acceptor distance. A donor−acceptor distance of less than 0.26 nm and an N−H···O angle of more than 120° were used as criteria for the identification of hydrogen bonds (Levitt & Sharon, 1988; Qi et al., 1994). The results are summarized in Table 4.

The RMSD value within the β-sheet region was very low, less than 0.05 nm for the backbone atoms, so that this region seems to be very rigid (Figure 11). The loop region Arg9-Glu14, connecting strands Tyr3-Leu7 and Thr15-Val19, in contrast, seems to be flexible as it shows a backbone RMSD value of 0.1 nm.

In addition to the β-sheet structures, three helical regions could be identified in Fd_{Se}, Ile25-Gly33, Asp66-Gly73, and

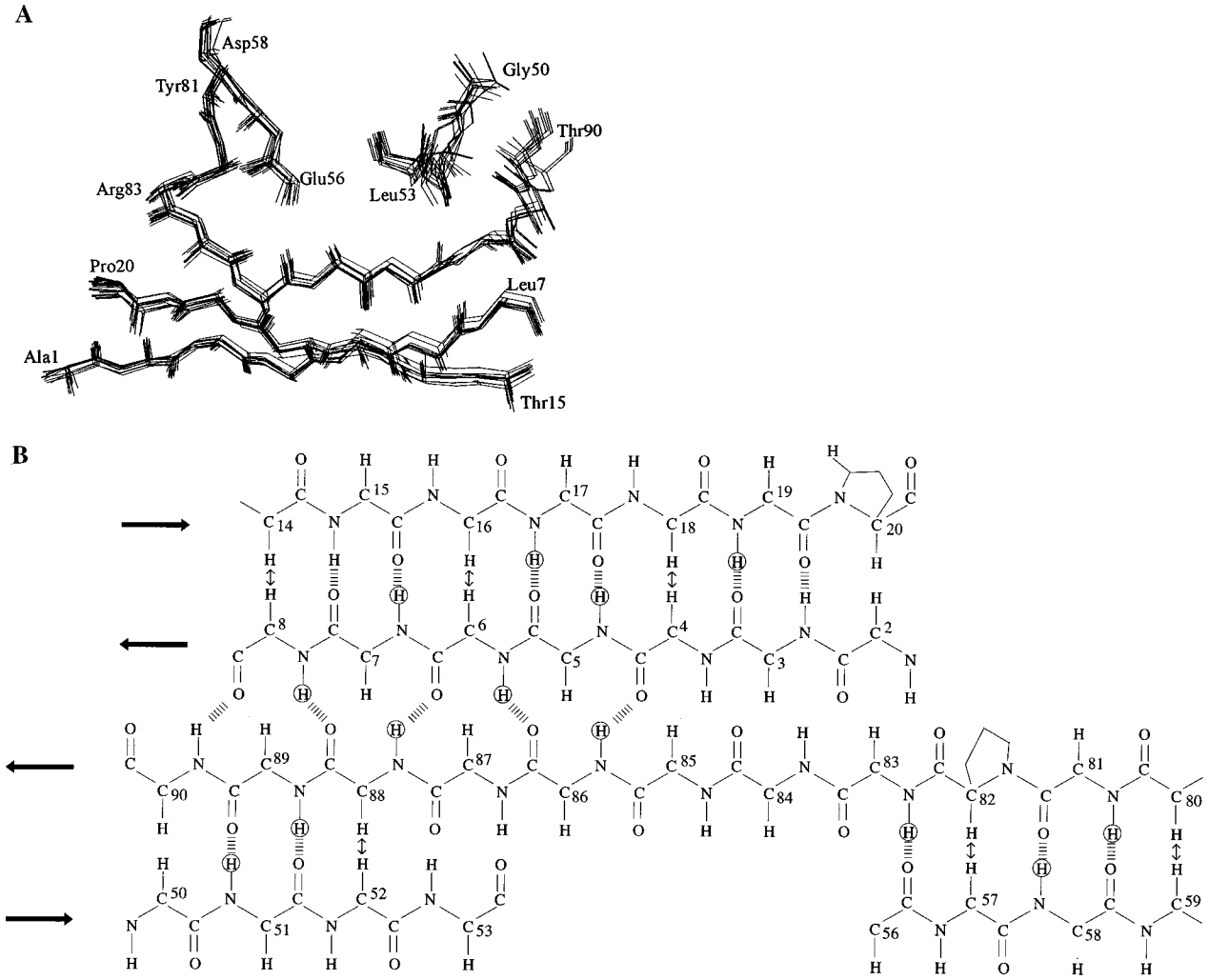

FIGURE 10: Detailed view of the β-sheet region of Fd_{Se}. The superposition (A) is shown for ten structures resulting from the molecular dynamics calculation. The schematic presentation (B) of the β-sheet region shows the hydrogen bonds involved in the formation of the secondary structure. Slow exchanging amide protons are marked by circles. NOEs that were observed between C_α-protons are indicated by arrows.

Glu93-Tyr97. According to the hydrogen bond analysis (Table 4), the first helix starts either with the hydrogen bond Val28-Ile25 or Ala29-Ile25, both of which have approximately the same number of occurence in the 20 structures from restrained MD calculations that we analyzed. From the proton/deuteron exchange experiments, however, it must be concluded that Val28 is involved in a strong hydrogen bond. Accordingly, the helix starts with the Val28-Ile25 hydrogen bond and proceeds with the Ala29-Leu26 hydrogen bond. These $i,i+3$ hydrogen bonds give the NH_2-terminus of the first helix 3_{10} character, whereas the subsequent $i,i+4$ hydrogen bonds (Glu31-Asp27, Gln32-Val28, Gly33-Ala29) indicate α-helical character. This helix is probably rather flexible, as no helix-typical $^3J_{NH_\alpha}$ coupling constant and only one slow exchanging proton could be observed. The same is true for the two other helices. A distinction between 3_{10}- and α-helix could not be made for the second helix (Asp66-Gly 73), whereas helix 3 (Glu93-Tyr 97) represents a single turn of a 3_{10}-helix (Table 4). The occurence of hydrogen bonds stabilizing the latter two helices was lower than for the NH_2-terminal helix. This may suggest that helix 2 and helix 3 are even more prone to structural fluctuations than helix 1.

The 50 structures obtained after restrained MD calculations were also analyzed for salt bridges (Table 4). The criterion used to define a salt bridge was a distance of less than 0.4 nm between the charged groups (Barlow & Thornton, 1983). No electrostatic interactions were introduced in the MD calculations, which may explain the low percentage of occurence of some of the salt bridges. The ion pair Lys51-Glu56, however, was present in all calculated structures.

Calculation of the accessible surface area for all amino acids can serve to define the non-exposed amino acids and thus can help to define the hydrophobic core of Fd_{Se}. The hydrophobic amino acids Val5, Leu7, Ile17, Val19, Ile25, Val28, Ala29, Gly50, Leu52, Gly55, Val57, Ile70, Gly73, Phe74, Ala80, Pro82, and Cys86 are not solvent accessible and are thus forming the hydrophobic core of the protein (Figure 12). The salt bridge Lys51-Glu56 is in the center of this core (Figure 13), whereas all other salt bridges observed are located at the protein surface. Also, the Cys86 side chain forms part of the core, explaining the low exchange rate of the thiol proton with the solvent protons observed in the NMR spectra. Both the hydrophobic core and the salt bridges are solely established from the NMR data, since electrostatic and hydrophobic interactions were not treated explicitly in the calculation procedure.

Quality of the Modeled Regions of the Protein. The modeling was intended to stabilize the correct backbone conformation in the cluster environment that is highly

Table 4: Hydrogen Bonds and Salt Bridges from Restrained MD Calculations[a]

N−H	C=O	occurrence
A. Hydrogen Bonds in β-Strands		
Tyr3	Val19	100%
Val5	**Ile17**	**100%**
Thr6	**Cys86**	**100%**
Leu7	**Thr15**	**100%**
Val8	**Ile88**	**100%**
Thr15	Leu7	100%
Ile17	**Val5**	**100%**
Val19	**Tyr3**	**100%**
Lys51	**Leu89**	**80%**
Asp58	**Tyr81**	**100%**
Tyr81	**Asp58**	**100%**
Arg83	**Glu56**	**100%**
Cys86	**Lys4**	**100%**
Ile88	**Thr6**	**55%**
Leu89	**Lys51**	**100%**
Thr90	Val8	100%
B. Hydrogen Bonds in α-Helices		
Val28	**Ile25**	**100%**
Ala29	Ile25	100%
Ala29	Leu26	100%
Glu31	Asp27	100%
Gln32	Val28	100%
Gly33	Val28	100%
Gly33	Ala29	100%
Leu34	Ala29	95%
Ile70	Asp66	100%
Glu71	Asp67	70%
Glu71	Asp68	80%
Lys72	Gln69	65%
Gly73	Ile70	80%
Leu96	Glu93	100%
Tyr97	Glu94	100%
C. Other Hydrogen Bonds		
Val79	Leu76	90%
Ala80	Leu76	70%
Ala80	Thr77	75%
Asn91	Arg9	100%

D. Salt Bridges

+ charge	− charge	occurrence
Lys4	Asp85	50%
Arg41	Asp35	60%
Lys51	Glu56	100%
Lys72	Glu95	80%
Arg83	Asp58	100%
Arg83	Asp67	65%

[a] The hydrogen bonds and salt bridges were deduced by the criteria given in the text from the 20 structures selected after the molecular dynamics calculations. Hydrogen bonds and salt bridges are listed in the table if their frequency of occurrence was equal to or higher than 50%. Hydrogen bonds that showed a slow exchange of the corresponding amide proton are indicated in bold letters.

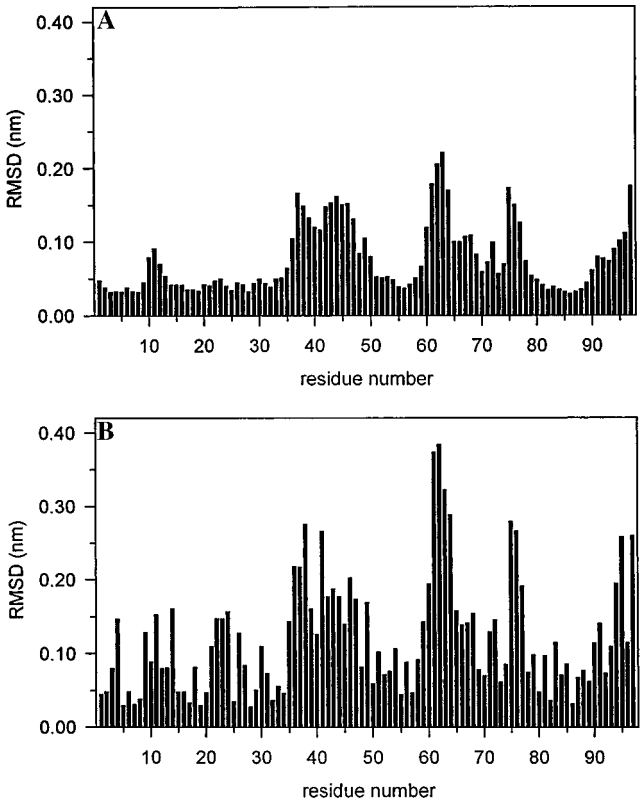

FIGURE 11: Quality of calculated structures. Diagrams of the RMSD values per residue for the 20 structures obtained after molecular dynamics calculations are shown. The RMSD values for the backbone atoms and all heavy atoms are shown in A and B, respectively.

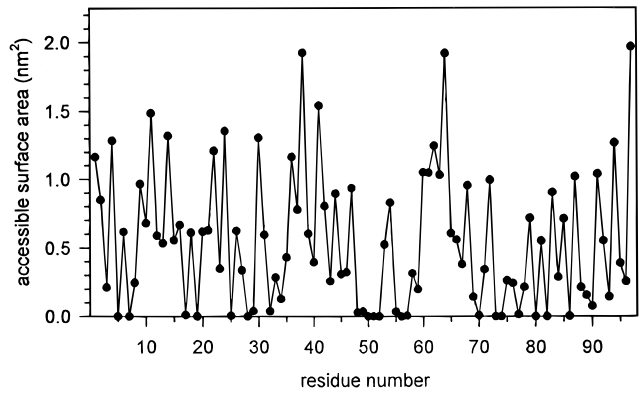

FIGURE 12: Solvent accessible surface area along the polypeptide chain. The accessible surface area was calculated by using a radius of 0.16 nm for a water molecule.

invariant among all [Fe_2S_2] ferredoxins. The 34 restraints (Table 2) deduced from crystal structures of homolgous ferredoxins were sufficient to produce a model that was consistent with all experimental data. Similar restraints were successfully applied in recent studies to determine structural models for putidaredoxin (Pochapsky et al., 1994) and Fd from *Synechocystis* (Lelong et al., 1995). A characterization of the cluster vicinity was not performed in our study, since the low number of restraints used for modeling does not allow a detailed analysis. Such analysis will only be possible on the basis of a crystal structure.

Comparison to the Structures of Homologous Ferredoxins. Overall, the solution structure of Fd_{Se} is very similar to the crystal structures of the homologous ferredoxins determined thus far. The β-sheet region of all ferredoxins is virtually identical, except for the short β-sheet formed by Tyr81-Arg83 and Glu56-Asp58 that is present in Fd_{Se} only.

The pattern of helical segments in Fd_{Se} is consistent with the structural elements deduced for crystal structures of *Anabaena* and *E. arvense* Fd and for the solution structure of *Synechocystis* Fd. Helices 2 and 3 were not detected in the crystal structures of *A. sacrum* and *S. platensis* Fd, both of which show high B-factors in the corresponding regions. Furthermore the helices cannot be safely deduced from the NMR data of *Anabaena* Fd (Oh & Markley, 1990). All these results are consistent with our observation of an increased flexibility of these helices as evidenced by increased $^3J_{HN_\alpha}$ coupling constants and fast amide proton exchange.

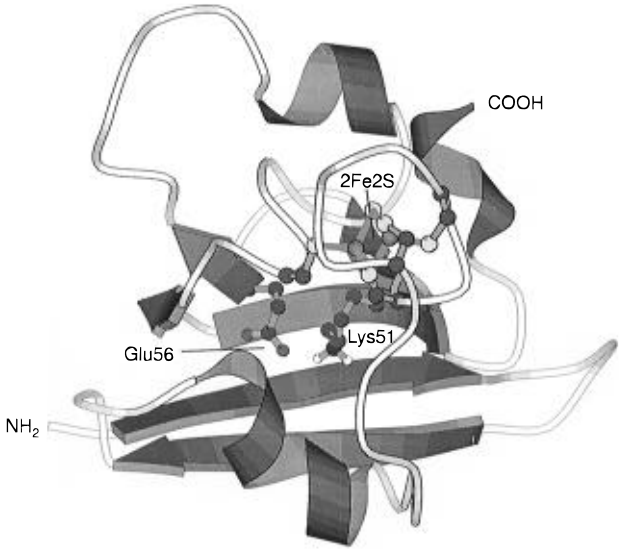

FIGURE 13: Location of the Lys51-Glu56 salt bridge. In this schematic MOLSCRIPT (Kraulis, 1991) presentation residues Lys51 and Glu56, the iron−sulfur cluster, and its ligating cysteines are shown in ball and stick representation.

The region Ser60-Phe64 is underdetermined by the NMR data in Fd_{Se} but is close to the cluster in the crystal structures of homologous ferredoxins, a fact that may explain the lack of observable resonances in this region. A structure of Fd_{Se} determined under the assumption of a C_α(Phe64)−Fe distance of less than 0.8 nm for either Fe ion with restrained MD calculations was entirely compatible with the NMR data, so that the assertion may be made that this loop region is identical in *Anabaena* and *S. elongatus* Fd as far as the relative location of loop and cluster is concerned. The rmsd value for the protein backbone atoms between the *Synechococcus* and *Anabaena* Fd except for Ser60-Phe64 region is 0.338 nm. Both proteins show a sequence homology of approximately 70% (Table 1).

Thermostability. This structure determination of a $[Fe_2S_2]$ ferredoxin from a thermophilic organism offers the opportunity to identify possible principles of thermostability.

Apart from the existence of a short, two-stranded β-sheet (Tyr81-Arg83 and Glu56-Asp58), no dramatic increase in secondary structure content of Fd_{Se} as compared to $[Fe_2S_2]$ ferredoxin from mesophilic organisms was observed. The hydrogen bonding pattern is also very conserved among all $[Fe_2S_2]$ ferredoxins investigated so far. Differences in the numbers of slowly exchanging amide protons between the ferredoxins from *S. elongatus*, *Synechocystis* (Lelong et al., 1995), and *Anabaena* (Chae et al., 1994) most probably can be attributed to the different conditions used for the exchange experiments.

The only additional clue to structural differences explaining the thermostability of Fd_{Se} is its unusually large hydrophobic core, consisting of 17 amino acids as compared to, for example, *A. sacrum* Fd that contains only a 7-amino acid hydrophobic core (Tsutsui et al., 1983). The internal salt bridge, Lys51-Glu56, is so far unique in $[Fe_2S_2]$ ferredoxins whose structures are known. In many ferredoxins, Glu56 is substituted with threonine or serine. As Fd_{Se} is the only thermostable protein among these, it may be suggested that the internal salt bridge is related to the thermostability of Fd_{Se}. Salt bridges have been related to thermostability before in general (Perutz, 1978; Ruegg et al., 1982) as well as in ferredoxins in particular (Perutz & Raidt, 1975; Hase et al., 1983). The importance of internal salt bridges for protein stability as opposed to surface salt bridges was stressed before (Waldburger et al., 1995), although evidence for unfavorable energetics of internal salt bridges was presented in several instances (Hendsch & Tidor, 1994).

Thus, a conclusive answer as to the origins of the thermostability of Fd_{Se} cannot be given at the present time. Nevertheless, our results support the observation that only minimal structural rearrangements are necessary to increase the thermostability of proteins.

ACKNOWLEDGMENT

We are grateful to Dr. A. Ejchart for help with the NMR spectrometers and to R. Hofmann and F. Herrmann for help with the computers.

SUPPORTING INFORMATION AVAILABLE

Table of ^1H resonance assignments of Fd_{Se} at pH 7.0, 298 K (3 pages). Ordering information is given on any current masthead page.

REFERENCES

Barlow, D. J., & Thornton, J. M. (1983) *J. Mol. Biol. 168*, 867−885.
Brünger, A. T. (1993) *X-PLOR Version 3.1*, Howard Hughes Medical Institute and Yale University, New Haven, CT.
Castenholz, R. W. (1969) *Bacteriol. Rev. 33*, 476−504.
Chae, Y. K., Abildgaard, F., Moobery, E. S., & Markley, J. L. (1994) *Biochemistry 33*, 3287−3295.
Clore, G. M., Groneborn, A. M., Nilges, M., & Ryan, C. A. (1987)- *Biochemistry 26*, 8012−8023.
Edmonds, C. G., & Smith, R. D. (1990) *Methods Emzymol. 193*, 412−431.
Englander, S. W., & Wand, A. J. (1987) *Biochemistry 26*, 5953−5958.
Ernst, R. R. (1992) *Angew. Chem. 104*, 817−852.
Fukuyama, K., Hase, T., Matsumoto, S., Tsukihara, T., Katsube, Y., Tanaka, N., Kakudo, M., Wada, K., & Matsubara, H. (1980) *Nature 286*, 522−524.
Güntert, P., & Wüthrich, K. (1992) *J. Magn. Reson. 96*, 403−407.
Hase, T., Matsubara, H., Koike, H., & Katoh, S. (1983) *Biochim. Biophys. Acta 744*, 46−52.
Hendsch, Z. S., & Tidor, B. (1994) *Protein Sci. 3*, 211−226.
Higgins, D. G., Bleasby, A. J., & Fuchs, R. (1992) *Comput. Appl. Biosci. 8*, 189−191.
Ikemizu, S., Bando, M., Sato, T., Morimoto, Y., & Tsukihara, T. (1994) *Acta Crystallogr. D50*, 167−174.
Kabsch, W., & Sander, C. (1983) *Biopolymers 22*, 2577−2637.
Knaff, D. B., & Hirasawa, M. (1991) *Biochim. Biophys. Acta 1056*, 93−125.
Koike, H., & Katoh, S. (1979) *Plant Cell Physiol. 20*, 1157−1161.
Kraulis, P. J. (1991) *J. Appl. Crystallogr. 24*, 976 - 980.
Kraulis, P. J., Clore, G. M., Nilges, M., Jones, T. A., Petterson, G., Knowles, J., & Gronenborn, A. M. (1989) *Biochemistry 28*, 7241−7257.
Krauss, N., Hinrichs, W., Witt, I., Fromme, P., Pritzkow, W., Dauter, Z., Betzel, C., Wilson, K. S., Witt, H. T., & Saenger, W. (1993) *Nature 361*, 326−331.
Lelong, C., Sétif, P., Bottin, H., André, F., & Neumann J.-M. (1995) *Biochemistry 34*, 14462−14473.
Levitt, M., & Sharon, R. (1988) *Proc. Natl. Acad. Sci. U.S.A. 85*, 7557−7561.
Marion, D., & Wüthrich, K. (1983) *Biochem. Biophys. Res. Commun. 113*, 967−974.
Matsubara, H., & Saeki, K. (1992) *Adv. Inorg. Chem. 38*, 223−280.
Meyer, J. (1988) *Trends Ecol. Evol. 3*, 222−226.
Neuhaus, D., Wagner, G., Vasak, M., Kägi, J. H. R., & Wüthrich, K. (1985) *Eur. J. Biochem. 151*, 257−273.

Nilges, M., Gronenborn, A. M., Brünger, A. T., & Clore, G. M. (1988a) *Protein Eng. 2*, 27−38.
Nilges, M., Clore, G. M., & Gronenborn, A. M. (1988b) *FEBS Lett. 239*, 129−136.
Oh, B. H., & Markley, J. L. (1990) *Biochemistry 29*, 3993−4004.
Perutz, M. (1978) *Science 201*, 1187−1191.
Perutz, M., & Raidt, H. (1975) *Nature 255*, 256−259.
Pochapsky, T. C., Ye, X. M., Ratnaswamy, G., & Lyons, T. A. (1994) *Biochemistry 33*, 6424−6432.
Powell, M. J. D. (1977) *Mathemat. Progr. 12*, 241−254.
Qi, P. X., Di-Stefano, D. L., & Wand, A. J. (1994) *Biochemistry 33*, 6408−6417.
Rousseau, F., Sétif, P., & Lagoutte, B. (1993) *EMBO J. 12*, 1756−1765.
Ruegg, C., Ammer, D., & Lerch, K. (1982) *J. Biol. Chem. 257*, 6420−6426.
Rypniewski, W. R., Breiter, D. R., Benning, M. M., Wesenberg, G., Oh, B., Markley, J. L., Rayment, I., & Holden, H. M. (1991) *Biochemistry 30*, 4126−4131.
Schatz, G. H., & Witt, H. T. (1984) *Photobiochem. Photobiophys. 7*, 1−14.
Shin, M., Sakihama, N., Koike, H., & Inoue, Y. (1984) *Plant Cell Physiol. 25*, 1575−1578.
Tsukihara, T., Fukuyama, K., Nakamura, M., Katsube, Y., Tanaka, N., Kakudo, M., Wada, K., Hase, T., & Matsubara, H. (1981) *Biochem. J. 90*, 1763−1773.
Tsukihara, T., Fukuyama, K., Mizushima, M., Harioka, T., Kusoniki, M., Katsube, Y., Hase, T., & Matsubara, H. (1990) *J. Mol. Biol. 216*, 399−410.
Tsutsui, T., Tsukihara, T., Fukuyama, K., Katsube, Y., Hase, T., Matsubara, H., Nishikawa, Y., & Tanaka, N. (1983) *J. Biochem. 94*, 299−302.
Van der Plas, J., de Groot, R. P., Woortman, M. R., Cremers, F., Borrias, M., van Arkel, G., & Weisbeck, P. (1988) *Photosynth. Res. 18*, 179−204.
Wagner, G., Braun, W., Havel, T. F., Schaumann, T., Go, N., & Wüthrich, K. (1987) *J. Mol. Biol. 196*, 611−639.
Waldburger, C. D., Schildbach, J. F., & Sauer, R. T. (1995) *Nat. Struct. Biol. 2*, 122−128.
Weber, N., & Strotmann, H. (1993) *Biochim. Biophys. Acta 1143*, 204−210.
Wishart, D. S., Sykes, B. D., & Richards, F. M. (1991) *J. Mol. Biol. 222*, 311−333.
Wishart, D. S., Sykes, B. D., & Richards, F. M. (1992) *Biochemistry 31*, 1647−1651.
Wüthrich, K. (1986) *NMR of Proteins and Nucleic Acids*, John Wiley & Sons, New York.
Wüthrich, K., Billeter, M., & Braun, W. (1983) *J. Mol. Biol. 169*, 949−961.
Yu, L., Zhao, J., Mühlenhoff, U., Bryant, D. A., & Golbeck, J. H. (1993) *Plant Physiol. 103*, 171−180.
Zanetti, G., & Merati, G. (1987) *Eur. J. Biochem. 169*, 143−146.

BI961144M